RESEARCH PAPER

Comparison between PSM and IBESS approaches for the fatigue life estimation of weldments

Federico Scacco[1] · Uwe Zerbst[2] · Giovanni Meneghetti[1] · Mauro Madia[2]

Abstract

In the framework of the fatigue assessment of welded components, several methods are available in design standards such as the nominal stress, hot-spot stress, notch stress and linear elastic fracture mechanics approaches. The present paper aims at comparing two advanced local approaches for the fatigue strength assessment of different welded joints made of steel. The first one is IBESS which is based on short crack fracture mechanics. The second one is the PSM which instead involves the strain energy density approach. Both methods will be briefly presented, and the fatigue life prediction results discussed. The results obtained for the joint geometries considered in this work show advantages and drawbacks of the approaches, which are thoroughly analysed as well.

Abbreviations

FAT	FAT class, endurable stress range at the reference number of cycles N_A and for survival probability 97.7%
FE	Finite element
FKM	Forschungskuratorium Maschinenbau
HAZ	Heat-affected zone
IBESS	Integrale Bruchmechanische Ermittlung der Schwingfestigkeit von Schweißverbindungen
IBESS FAT	FAT class obtained with IBESS
IIW	International Institute of Welding
IIW FAT	FAT class reported in IIW recommendations for classified details [1]
MAG	Metal active gas (welding)
PSM	Peak stress method
PSM FAT	FAT class according to the PSM, i.e. range of the endurable equivalent peak stress $\Delta\sigma_{eq,peak}$ for a probability of survival 97.7% at N_A (PSM FAT = 156 MPa)
PSM FAT$_{nom}$	FAT class in terms of range of the applied nominal stress derived from PSM FAT
PWHT	Post-weld heat treatment
NSIFs	Notch stress intensity factors
SED	Strain energy density
TIG	Tungsten inert gas (welding

Nomenclature

a_{ref}:	Reference dimension for selecting the maximum FE size d for the application of the PSM
a:	Crack depth
a_i:	Initial crack depth
C:	Parameter in the crack propagation law
c_{wi}:	Coefficients accounting for mean stress effect of ith loading mode ($i = 1, 2$ or 3)
d:	Average FE size of the adopted free mesh pattern
d_{max}:	Maximum FE size for the PSM application
d_{SED}:	FE size inside the structural volume R_0 adopted for the SED calculation
da/dN:	Fatigue crack propagation rate

✉ Giovanni Meneghetti
giovanni.meneghetti@unipd.it

[1] Department of Industrial Engineering, University of Padova, via Venezia, 135131 Padova, Italy

[2] Bundesanstalt Für Materialforschung Und -Prüfung (BAM), Unter den Eichen 87, 12205 Berlin, Germany

e_i:	Coefficients for calculating $\Delta\overline{W}$ as function of 2α and ν ($i=1, 2$ or 3)
E:	Young's modulus
E':	$= E$ For plane stress and $E/(1-\nu^2)$ for plane strain conditions
$f(R)$:	Mean stress correction according to IIW
f_{wi}:	Coefficients for calculating $\sigma_{eq,peak}$ ($i=1, 2$ or 3)
h:	Reinforcement height
J:	J-Integral (monotonic loading)
k:	Slope of finite life fatigue ($S-N$) curve in double logarithmic scale
K_i:	NSIF parameters relevant to opening, sliding and tearing loading modes ($i=1, 2$ or 3)
$K_{FE}^*, K_{FE}^{**}, K_{FE}^{***}$:	Non-dimensional NSIF parameters based on the PSM
l:	Root face length
L:	Weld width
m:	Exponent in fatigue crack propagation law
N:	Number of loading cycles
N_A:	Reference number of loading cycles equal to 2×10^6
N_f:	Number of cycles to failure
p:	Fitting exponent of the second term in the crack propagation law
PS:	Probability of survival
R:	Stress ratio ($\sigma_{min}/\sigma_{max}$)
R_0:	Size of structural volume in which the SED is averaged
r, θ, z:	Coordinates of cylindrical reference system
s:	Index to identify adjacent vertex nodes for the application of the PSM in 3D FE models
S:	Stress
T:	Plate thickness
T_σ:	Scatter index
U:	Crack closure factor ($\Delta K_{eff}/\Delta K$)
U_{LC}:	Crack closure factor for long cracks
U_{SC}:	Crack closure factor for short cracks
z:	Weld leg length in cruciform joints and longitudinal gussets
2α:	Opening angle of a sharp notch
Δa:	Crack extension
$\Delta\varepsilon_{ref}$:	Reference strain range
ΔJ:	Cyclic J-integral ($\neq J_{max} - J_{min}$)
ΔK:	Stress intensity factor range ($= K_{max} - K_{min}$)
ΔK_{eff}:	Effective K-factor range
ΔK_p:	Plasticity-corrected ΔK
ΔK_{th}:	Fatigue crack propagation threshold
$\Delta K_{th,eff}$:	Intrinsic fatigue crack propagation threshold (no crack closure effect)
$\Delta K_{th,LC}$:	Fatigue crack propagation threshold in the long crack regime
$\Delta K_{th,SC}$:	Fatigue crack propagation threshold in the (physically) short crack regime
ΔL_r:	Ligament yielding parameter for cyclic loading
$\Delta\overline{W}$:	Averaged SED range
$\Delta\overline{W}_{FEM}$:	Averaged SED range calculated from the FE model
$\Delta\sigma$:	Stress range (maximum value minus minimum value)
$\Delta\sigma_{app}$:	Applied stress range (refers to cross section without crack)
$\Delta\sigma_{nom}$:	Nominal stress range
$\Delta\sigma_{eq,peak}$:	Equivalent peak stress range according to the PSM
$\Delta\sigma_{eq,peak,PSM}$:	Equivalent peak stress range calculated applying the PSM
$\Delta\sigma_{eq,peak,SED}$:	Equivalent peak stress range calculated starting from the SED
$\overline{\Delta\sigma_{eq,peak,PSM}}$:	Average equivalent peak stress range calculated applying the PSM
$\overline{\Delta\sigma_{eq,peak,SED}}$:	Average equivalent peak stress range calculated starting from the SED
$\Delta\sigma_{ij,peak}$:	Peak stress range for opening or sliding or tearing local stresses
$\overline{\Delta\sigma_{ij,peak}}$:	Average peak stress range for opening or sliding or tearing local stresses
$\Delta\sigma_{ref}$:	Reference stress range
σ:	Stress
σ_0:	Reference yield stress
$\sigma_{11,peak}$:	Maximum principal peak stress
σ_a:	Stress amplitude ($= \Delta\sigma/2$)
σ_{nom}:	Nominal stress
σ_Y:	Yield stress
λ_i:	Stress singularity degrees relevant to opening, sliding and tearing loading modes ($i=1, 2$ or 3)
ν:	Poisson's ratio
ρ:	Weld toe radius
$\sigma_{eq,peak}$:	Equivalent peak stress according to the PSM
$\sigma_{\theta\theta,\theta=0,peak}$:	Linear elastic opening (mode I) peak stress calculated at notch tip by FE analysis for applying the PSM

$\tau_{r\theta,\theta=0,\text{peak}}$: Linear elastic sliding (mode II) peak stress calculated at notch tip by FE analysis for applying the PSM

$\tau_{\theta z,\theta=0,\text{peak}}$: Linear elastic tearing (mode III) peak stress calculated at notch tip by FE analysis for applying the PSM

1 Introduction

The aim of the present paper is a comparison of two methods for the prediction of the fatigue strength of weldments. The peak stress method (PSM) has been developed at the University of Padova [1, 2], and it is an engineering FE-oriented tool for the rapid estimation of notch stress intensity factors (NSIFs) thanks to the use of coarse 2D or 3D FE analyses. The PSM applies to weldments at the weld toe and weld root, whose geometry is idealised as sharp V-notches with null radius. Due to the sharp V-notches, external loads generate singular stress fields that can be used for the estimation of the time spent for initiation and propagation of a small crack in the vicinity of the V-notch tip. In principle, any fatigue model based on NSIFs can take advantage of the PSM and in the present investigation the PSM is complemented by the strain energy density (SED) approach for the fatigue strength assessment of welded joints.

The IBESS method has been developed, among others, at BAM Berlin [3, 4] for the determination of the fatigue life of welded joints based on short crack fracture mechanics. For the application to weldments with cracks originating at the weld toe, parametrized analytical solutions as a function of the local weld toe geometry are provided for input data such as the stress profile in wall thickness direction. Other special features are an option for establishing an initial crack size based on a crack arrest criterion and the treatment of multiple cracks at stress levels above the endurance limit.

Both methods and the nominal stress approach according to IIW are applied to 10 data sets of three different weldment types, two materials and as-welded as well as post-weld heat treated conditions. This will be exercised in Section 3. In the next sections, brief introductions are given to the nominal stress approach (Section 2.1), PSM (Section 2.2) and IBESS (Section 2.3).

2 Approaches for the fatigue assessment of weldments

2.1 Conventional nominal stress approach

A widely used approach for the assessment of cyclically loaded weldments is the nominal stress approach based on

FAT classes, whereby FAT is the acronym for "fatigue". FAT classes are predefined fatigue strength values in terms of stress range of an S–N curve at $N = 2 \times 10^6$ loading cycles. Each class is lowered by certain and fix percentage. The principle is illustrated in Fig. 1.

Documents such as the IIW guideline [5], the Eurocode [6] or the FKM guideline [7] contain FAT classes of structural details obtained on experimental basis. If the FAT class of a weld in a structure is known, the complete S–N curve can be constructed. The finite life branch is assumed to have a slope k of 3 for normal stress perpendicular to the weld seam and it passes through the point defined by the FAT class.

In case of IIW recommendations, the finite life branch of the S–N curve is terminated at 10^7 cycles where it passes into either the endurance limit or a very high cycle fatigue branch with a slope of, e.g. 22 [5]. Eurocode 3 instead defines the constant amplitude fatigue limit at $N = 5 \times 10^6$ loading cycles, while for variable amplitude spectra, the fatigue strength has to be assessed basing on extended curves with a slope $k = 5$ up to $N = 10^8$ loading cycles.

Note that IIW, Eurocode and FKM use the same FAT diagrams, but they differ in the stress ratio $R = \sigma_{\min}/\sigma_{\max}$ which they use as their basis: $R = 0.5$ for IIW; $R = 0$ for Eurocode; $R = -1$ for FKM. The discrepancy is compensated by different mean stress corrections. No detailed discussion on this will be provided here since only the IIW approach will be applied (see, however [8]). IIW uses the following expressions:

$$f(R) = \begin{cases} 1.6 & \text{for } R < -1 \\ -0.4 \cdot R + 1.2 & \text{for } -1 \leq R \leq 0.5 \\ 1 & \text{for } R > 0.5 \end{cases} \quad (1a)$$

$$f(R) = \begin{cases} 1.3 & \text{for } R < -1 \\ -0.4 \cdot R + 0.9 & \text{for } -1 \leq R \leq -0.25 \\ 1 & \text{for } R > -0.25 \end{cases} \quad (1b)$$

Equation 1a is valid for unwelded base material, wrought components with negligible residual stresses (lower than $0.2\sigma_Y$) and stress-relieved welded joints; Eq. 1b is reported to be valid for small-scale thin-walled welded components containing short welds. For complex two- or three-dimensional cases with global residual stresses and thick-walled components, it is suggested that $f(R) = 1$ is to be used [5].

In the general case, $f(R) = 1$ should not be exceeded. Note that the FAT classes are given in terms of the stress range $\Delta\sigma$, and not the stress amplitude σ_a (as it is

Fig. 1 Nominal stress approach based on FAT classes and principle
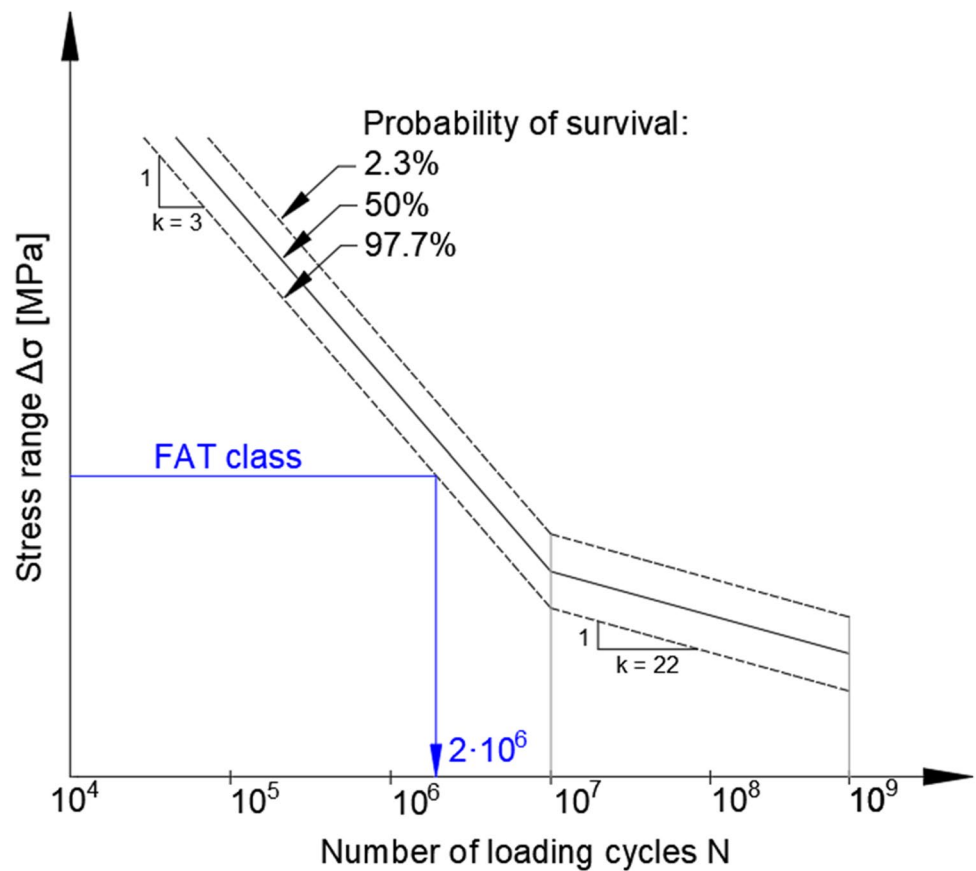
frequently the case in conventional fatigue) and a lower percentile value of probability of survival $PS = 97.7\%$.

2.2 The PSM

The peak stress method (PSM) is a finite element (FE)–based method to rapidly estimate notch stress intensity factors (NSIFs) K_1, K_2 and K_3 for the three loading modes at a sharp V-shaped notch, like for example in the case of a tube-to-flange welded joint reported in Fig. 2a. By means of a linear-elastic FE analysis with a relatively coarse mesh, the method correlates the peak stresses evaluated at the V-notch tip with NSIFs, by means of non-dimensional coefficients according to the following relationships:

$$K_{FE}^* = \frac{K_1}{\sigma_{\theta\theta,\theta=0,peak} \cdot d^{1-\lambda_1}} \text{(opening mode)} \tag{2}$$

$$K_{FE}^{**} = \frac{K_2}{\tau_{r\theta,\theta=0,peak} \cdot d^{1-\lambda_2}} \text{(sliding mode)} \tag{3}$$

$$K_{FE}^{***} = \frac{K_3}{\tau_{\theta z,\theta=0,peak} \cdot d^{1-\lambda_3}} \text{(tearing mode)} \tag{4}$$

In the previous equations, the parameter d is the average element size of the adopted FE free mesh which typically the FE analyst has to input before running the free mesh generation algorithm of the employed FE software; λ_i are stress singularity degrees which depend on the opening angle 2α of the V-notch [9, 10]; $\sigma_{\theta\theta,\theta=0,peak}$, $\tau_{r\theta,\theta=0,peak}$ and $\tau_{\theta z,\theta=0,peak}$ are the peak stresses defined in the local cylindrical coordinate system and evaluated at the node located at the V-notch tip; as an example, $\sigma_{\theta\theta,\theta=0,peak}$ means the opening stress acting in the direction normal to the notch bisector (see Fig. 2b).

K_1, K_2 and K_3 are NSIFs related to opening, sliding and tearing loading modes respectively, originally defined by Gross and Mendelson [11] with the following equations:

$$K_1 = \sqrt{2\pi}\lim_{r\to 0}[(\sigma_{\theta\theta})_{\theta=0} \cdot r^{1-\lambda_1}] \tag{5}$$

$$K_2 = \sqrt{2\pi}\lim_{r\to 0}[(\tau_{r\theta})_{\theta=0} \cdot r^{1-\lambda_2}] \tag{6}$$

$$K_3 = \sqrt{2\pi}\lim_{r\to 0}[(\tau_{\theta z})_{\theta=0} \cdot r^{1-\lambda_3}] \tag{7}$$

relative to the cylindrical coordinate system depicted in Fig. 2b. The linear elastic local stress components $\sigma_{\theta\theta}$, $\tau_{r\theta}$ and $\tau_{\theta z}$ are calculated close to the notch tip ($r \to 0$) and along

Fig. 2 **a** Assumption of the NSIF-based approach in fatigue design of welded joints. Example of a partial penetration tube-to-flange welded joint. The sharp V-notch opening angle 2α is typically 0° at the weld root and 135° at the weld toe. The circularly shaped structural volume of radius R_0 is centred at the weld toe or at the weld root according to the averaged SED approach. **b** Cylindrical reference system (r, θ, z) centred at the weld toe and local stress components
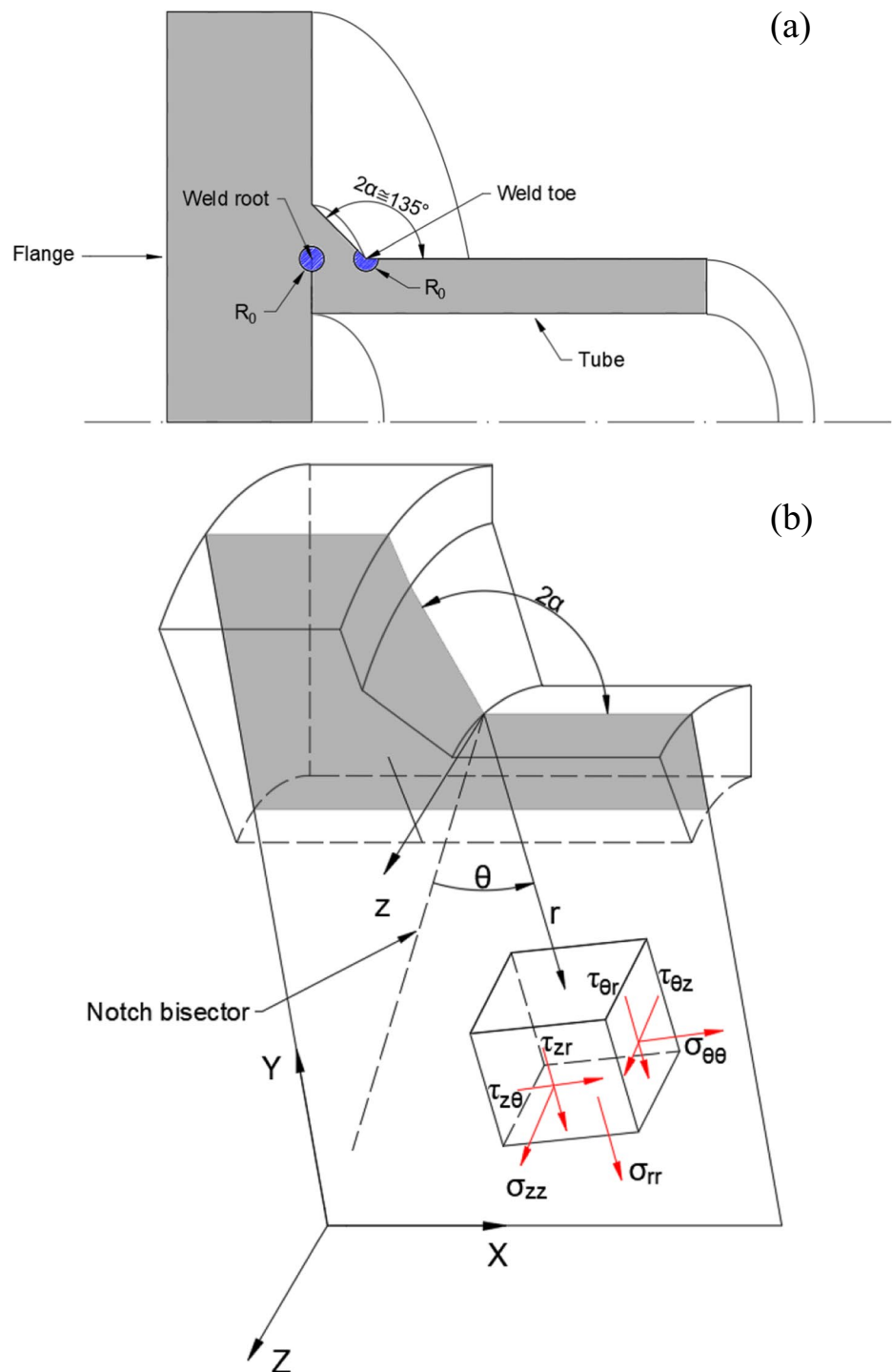
the notch bisector line ($\theta = 0$). The evaluation of NSIFs by applying definitions (5–7) is typically a burdensome procedure because it requires very fine FE mesh patterns to calculate accurately the local stress field at the V-notch tip [12]. Conversely, the PSM requires significantly coarser FE mesh patterns and therefore provides a tool for the rapid estimation of NSIFs.

The non-dimensional coefficients K^*_{FE}, K^{**}_{FE} and K^{***}_{FE} of Eqs. (2–4) have been originally calibrated for 2D finite elements [1, 13, 14]; afterwards, calibration has been extended to 3D FE models [15–17] and to commercial FE software packages other than Ansys [18]. A comprehensive review of the PSM has been reported recently [2] to which the reader is referred for the operating instructions to apply the PSM

within its range of applicability, which will be recalled later on.

The PSM being a method for an approximate, rapid, FE-oriented evaluation of the NSIFs, any fatigue strength criterion based on the NSIFs can in principle take advantage of the PSM. In particular, the PSM has been applied to the fatigue model based on the strain energy density (SED) averaged over a circular-shaped structural volume of radius R_0, as shown in Fig. 2a. According to Lazzarin et al. [19–21], the averaged SED over a structural volume $\Delta \overline{W}$ can be used as damage parameter for the fatigue strength assessment of weldments and calculated with the following expression based on the NSIFs:

$$\Delta \overline{W} = c_{w1} \frac{e_1}{E} \left(\frac{\Delta K_1}{R_0^{1-\lambda_1}} \right)^2 + c_{w2} \frac{e_2}{E} \left(\frac{\Delta K_2}{R_0^{1-\lambda_2}} \right)^2 + c_{w3} \frac{e_3}{E} \left(\frac{\Delta K_3}{R_0^{1-\lambda_3}} \right)^2 \tag{8}$$

In the previous equation, E is the material modulus of elasticity and parameter e_i depends on the opening angle 2α and Poisson's ratio ν. R_0 is the radius of the circular-shaped structural volume which has been found equal to 0.28 mm by Livieri and Lazzarin [19] in the case of steel weldments with weld toe failure. To take into account the effect of misalignments on the weldment, Fischer et al. [22] reviewed the SED approach and concluded an increased R_0 at the weld toe, i.e. 0.32 mm.

It is possible to equal the expression of the averaged SED valid for a triaxial stress state, Eq. 8, with the expression of the SED for an equivalent uniaxial plane strain state:

$$\Delta \overline{W} = \frac{1 - \nu^2}{2E} \cdot \Delta \sigma_{eq,peak}^2 \rightarrow \Delta \sigma_{eq,peak} = \sqrt{\frac{2 \cdot E \cdot \Delta \overline{W}}{1 - \nu^2}} \tag{9}$$

By substituting Eq. 8 in Eq. 9, the equivalent peak stress can be made explicit according to the following expression [2]:

$$\Delta \sigma_{eq,peak,PSM} = \sqrt{c_{w1} \cdot f_{w1}^2 \cdot \Delta \sigma_{\theta\theta,\theta=0,peak}^2 + c_{w2} \cdot f_{w2}^2 \cdot \Delta \tau_{r\theta,\theta=0,peak}^2 + c_{w3} \cdot f_{w3}^2 \cdot \Delta \tau_{\theta z,\theta=0,peak}^2} \tag{10}$$

The coefficient c_{wi} accounts for the mean stress effect; therefore, their values depend on the load ratio R_i of the relevant loading mode ($i = 1, 2$ or 3) [2]:

$$c_{wi}(R_i) = \begin{cases} \frac{1 + R_i^2}{(1 - R_i)^2} & \text{if stress relieved and} -1 \leq R_i \leq 0 \\ \frac{1 - R_i^2}{(1 - R_i)^2} & \text{if stress relieved and } 0 \leq R_i < 1 \\ 1 & \text{if as welded for any } R \text{ value} \end{cases} \tag{11}$$

In Eq. 10, parameters f_{wi} depend on the opening angle 2α and the Poisson's ratio ν, the average finite element size

d adopted in the FE analyses and the material structural volume with size defined by R_0. The expressions of f_{wi} are as follows [2]:

$$f_{w1} = K_{FE}^* \sqrt{\frac{2e_1}{1 - \nu^2}} \cdot \left(\frac{d}{R_0} \right)^{1-\lambda_1} \tag{12}$$

$$f_{w2} = K_{FE}^{**} \sqrt{\frac{2e_2}{1 - \nu^2}} \cdot \left(\frac{d}{R_0} \right)^{1-\lambda_2} \tag{13}$$

$$f_{w3} = K_{FE}^{***} \sqrt{\frac{2e_3}{1 - \nu^2}} \cdot \left(\frac{d}{R_0} \right)^{1-\lambda_3} \tag{14}$$

Eigenvalues λ_i and parameters e_i are reported in the literature for a range of opening angles [2]. However, since the opening angles of the weldments reported in the present investigations are different from the exemplary ones reported elsewhere [2], f_{wi} has been calculated for each opening angle 2α using Eqs. (12–14).

The PSM has been originally formalised for V-notch opening angles $2\alpha \leq 135°$, and coefficients K_{FE}^*, K_{FE}^{**} and K_{FE}^{***} are valid within the error in NSIFs estimations defined in [2]. When $2\alpha > 135°$, Eqs. (2–4) of the PSM cannot be applied, strictly speaking. In such circumstances, the SED parameter can be calculated directly from a FE analysis ($\Delta \overline{W}_{FEM}$) according to Eq. 15:

$$\Delta \overline{W}_{FEM} = \frac{\sum_{V(R_0)} \Delta W_{FEM,i}}{V(R_0)} \tag{15}$$

where the strain energy density $\Delta W_{FEM,i}$ is evaluated at the integration points of the ith finite element included in the structural volume (or area in 2D problems) having radius R_0. Then, the equivalent peak stress can be evaluated by means of Eq. 9, where now $\Delta \overline{W}$ must be interpreted as $\Delta \overline{W}_{FEM}$ according to the so-called direct approach.

In what follows, all weldments tested in the IBESS project and considered later on in the present paper have angles greater than 135°. More precisely, butt joints have $2\alpha = 148°$ and 155°, cruciform joints have $2\alpha = 143°$ and longitudinal gussets have $2\alpha = 146°$. Bearing this in mind, for butt and cruciform joints, the equivalent peak stress has been calculated from $\Delta \overline{W}_{FEM}$ by using the direct approach (Eq. 9 with $\Delta \overline{W} = \Delta \overline{W}_{FEM}$), while for the longitudinal gussets, it has been calculated using the PSM by means of Eq. 10. Whatever the notch opening angle, the equivalent peak stress obtained both from Eq. 9 with $\Delta \overline{W} = \Delta \overline{W}_{FEM}$ and from Eq. 10 has been systematically compared. The equivalent peak stress calculated by means of Eq. 9 with $\Delta \overline{W} = \Delta \overline{W}_{FEM}$ has been reported as $\Delta \sigma_{eq,peak,SED}$.

The master scatter band of the PSM has been originally calibrated on approximately 180 experimental data taken

from the literature and relevant to welded steel joints with weld toe failures ($2\alpha \cong 135°$) [23]. The welded joints had very different geometries and size and were subjected to simple axial or bending loadings. Figure 3 reports the master scatter band of the PSM along with approximately 860 experimental data (in terms of $\Delta\sigma_{eq,peak}$) relevant to weld toe as well as weld root failures, which enabled to validate systematically the PSM [2]. The scatter index T_σ resulted equal to 1.90 referred to probabilities of survival of 2.3 to 97.7%. It is worth mentioning that the scatter index of 1.90 is consistent with $T_\sigma = 1.50$ referred to probabilities of survival of 10 to 90%, which was found for single test series by Haibach [24]; this outcome supports the conclusion that the PSM fully accounts for the different geometries, sizes and loading mode, and the curves reported in Fig. 3 are master fatigue curves for different probabilities of survival.

2.3 The IBESS approach

The IBESS approach uses short crack fracture mechanics to determine the *S–N* curve and the endurance limit. It is characterized by four main features: (a) the elastic–plastic determination of the cyclic crack driving force, (b) the consideration of the gradual build-up of the crack closure phenomenon, (c) a crack arrest–based criterion for determining a fatigue strength relevant initial crack size for the fracture mechanics analysis and (d) multiple crack analyses for stress levels above the endurance limit. Only the most important aspects will be presented here. For a comprehensive overview of the methodology, the reader is referred to [3, 4].

2.4 Elastic–plastic determination of the cyclic crack driving force

An elastic–plastic crack driving force is necessary because mechanically short cracks are considered. "Mechanically short" means that the crack size is in the order of the plastic zone ahead of its tip. In IBESS, a "plasticity-corrected" cyclic stress intensity factor ΔK_p is determined which is a formally to ΔK transferred cyclic *J*-integral ΔJ.

$$\Delta K_p = \sqrt{\Delta J \cdot E'} \tag{16}$$

ΔJ is obtained by

$$\Delta J = \Delta K^2 / E' \cdot \left[f(\Delta L_r) \right]^{-2} \tag{17}$$

The yielding parameter ΔL_r is determined as

$$\Delta L_r = \Delta\sigma_{app} / \left(2 \cdot \sigma_0 \right) \tag{18}$$

with $\Delta\sigma_{app}$ being the applied stress range (cross section without crack) and σ_0 a reference yield stress for which analytical expressions for weldments are provided in IBESS. The $f(L_r)$ function follows the highest analytical options of R6 [25] and the British standard BS7910 [26]:

$$f(\Delta L_r) = \left[\frac{E \cdot \Delta\varepsilon_{ref}}{\Delta\sigma_{ref}} + \frac{1}{2} \frac{\Delta L_r^2}{E \cdot \Delta\varepsilon_{ref} / \Delta\sigma_{ref}} \right]^{-\frac{1}{2}} \tag{19}$$

however, modified for cyclic loading. An important point is that different to $\Delta K = K_{max} - K_{min}$ the cyclic *J* integral $\Delta J \neq J_{max} - J_{min}$. Instead, the Δ has to be applied to

Fig. 3 Fatigue assessment according to the PSM of weld toe and weld root failures in welded joints made of structural steel tested in as-welded or stress-relieved conditions (from [2])
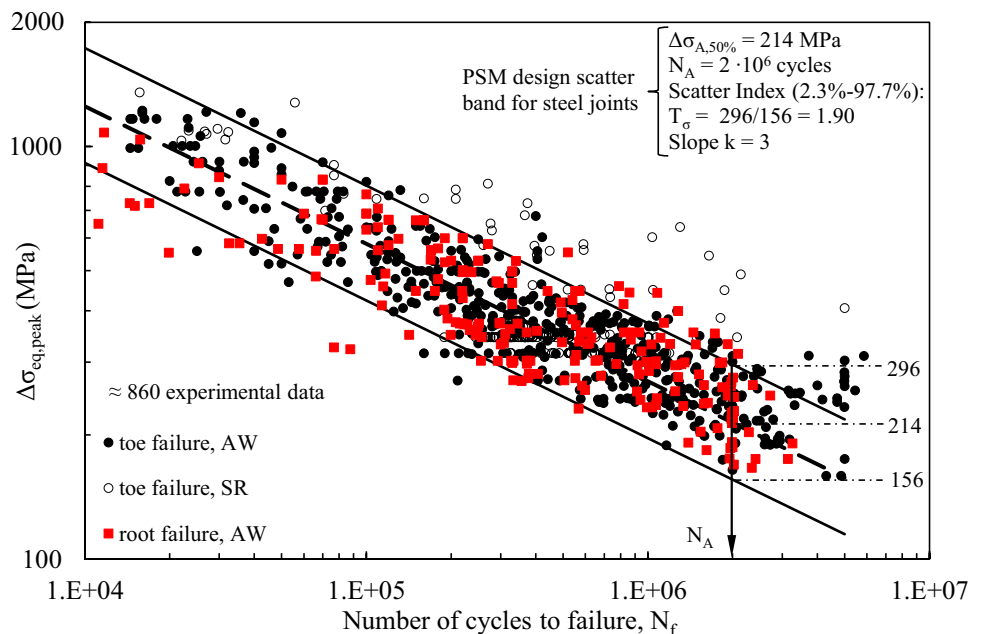
the arguments $\Delta\varepsilon_{ref}$, $\Delta\sigma_{ref}$ and $\Delta\sigma_{app}$. The factor 2 in the denominator of Eq. 18 takes into account the stress–strain hysteresis for materials showing symmetric behaviour in tension and compression.

2.5 Consideration of the gradual build-up of the crack closure phenomenon

Crack closure means the premature contact of the crack faces during unloading in the loading cycle. The phenomenon is caused by a number of different mechanisms. In plasticity-induced closure, the plastic zone ahead of the crack remains into the crack wake when the crack grows. This causes geometrical mismatch of the crack faces. Roughness-induced closure is caused by the asperity of the crack faces and enhanced by crack kinking or branching. Oxid-induced closure occurs when a material is prone to corrosion. At low mean stresses or R ratios, the oxide layer is partially rubbed off by friction when the crack is closed. The material corrodes again this way creating a corrosion debris which grows to a thickness much larger than the original layer. There exist further crack closure mechanisms which shall not be discussed here, but can be examined elsewhere [27].

The crack closure phenomenon is usually characterized by a crack closure parameter $U = \Delta K_{eff}/\Delta K$ where ΔK_{eff} characterizes the part of ΔK over which the crack is open. The crack closure phenomenon requires a certain extension of the crack wake. This is the reason why it is not existent at the beginning when the crack initiates, e.g. at a material defect: $U = 1$. During the stage of physically short crack propagation, the crack closure effects gradually build up

and U decreases until the crack becomes a long one, where eventually U becomes independent of the crack length as illustrated in Fig. 4.

In IBESS, the curve of Fig. 4 is determined by the following expression:

$$\frac{1 - U_{SC}(a)}{1 - U_{LC}} = \frac{\Delta K_{th,SC}(a) - \Delta K_{th,eff}}{\Delta K_{th,LC} - \Delta K_{th,eff}} \tag{20}$$

In the background is the assumption that the function $U_{SC}(a)$ is mirrored in the cyclic R-curve (Fig. 5).

In Eq. 20, U_{LC} is the crack size independent long crack closure parameter determined by the NASGRO approach [28], U_{SC} is its crack size dependent short crack equivalent, $\Delta K_{th,eff}$ is the intrinsic (closure free) component of the fatigue crack propagation threshold and $\Delta K_{th,SC}(a)$ is the cyclic R-curve, i.e. the fatigue crack propagation threshold which increases with crack extension. With respect to the determination of the cyclic R curve, the reader is referred to [3, 4] and [29].

2.6 Crack arrest–based determination of the initial crack size

This is based on a cyclic R-curve analysis, the principle of which is illustrated in Fig. 6. It combines three pieces of information. First, the cyclic R-curve is introduced (red line). Its origin is fixed by the initial crack depth a_i at the abscissa and the intrinsic threshold $\Delta K_{th,eff}$ at the ordinate. Finally, cyclic crack driving force curves $\Delta K_p - a$ are plotted for different applied loads $\Delta\sigma_1$ to $\Delta\sigma_3$.

Fig. 4 Schematic crack size dependency of the closure factor U [4]
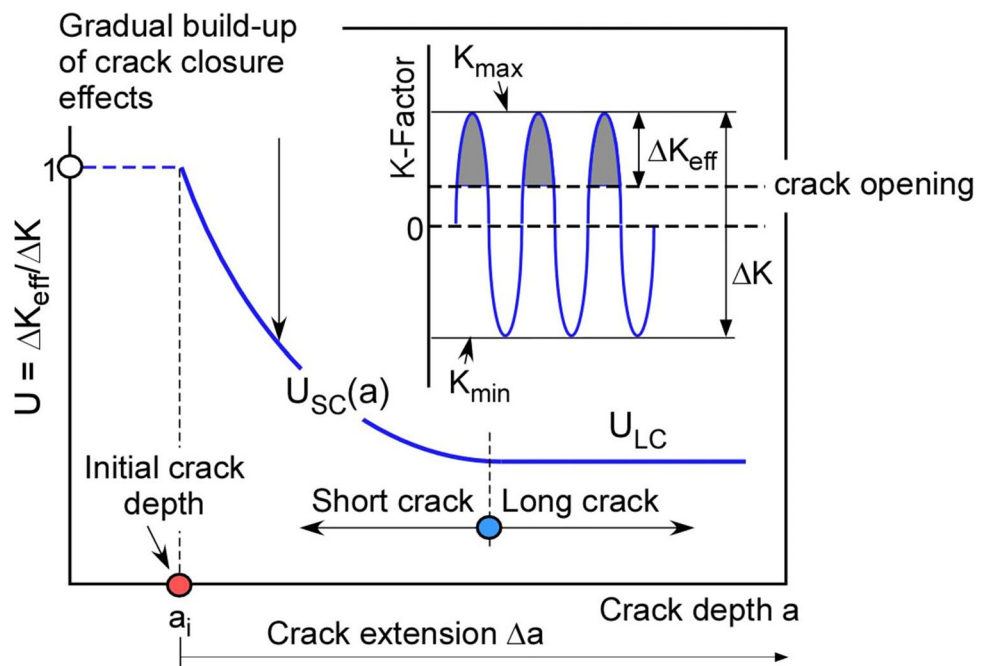
Fig. 5 Parallel development of the short crack closure parameter U_{SC} (left) and the cyclic R-curve (right), schematic view [4]
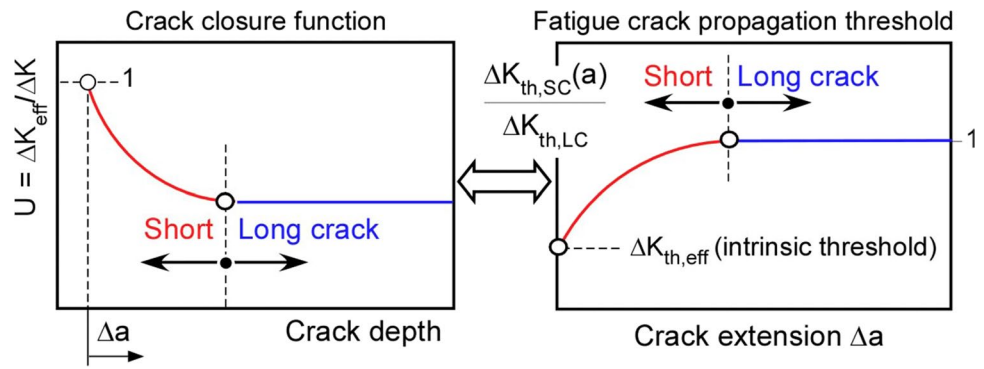
Fig. 6 Schematic view of a cyclic R-curve analysis. The transition from arrest to continuous growth is given by that crack driving force curve (referring to the load $\Delta\sigma_2$ in the example) which tangentially touches the cyclic R-curve [4]
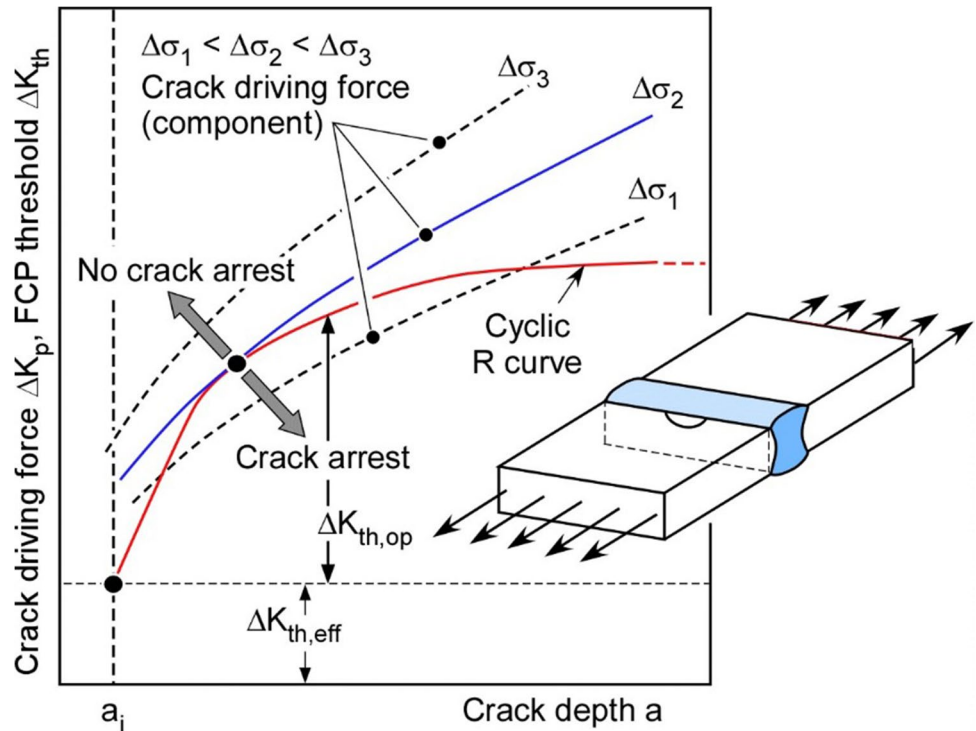
That curve which tangentially touches the cyclic R-curve (in the example $\Delta\sigma_2$) marks the transition from crack arrest to continuous crack propagation, in other words, the endurance limit. If the initial crack size a_i is known, the scheme can be applied to the determination of the endurance limit of components.

Vice versa, the principle can be used for the determination of a_i. To that purpose, the crack driving force curve $\Delta K_p - a$ is determined for a tensile plate with a semi-circular crack of varying size loaded at the endurance limit. The cyclic R-curve is still fixed by $\Delta K_{th,eff}$ at the ordinate but can be shifted at the abscissa. If this is done such that the crack driving force curve and the R-curve touch tangentially, a_i can be taken from the diagram. It is the size of the crack which later on would just arrest at the stress level of the plain (or material)

endurance limit. Actually, this provides a lower bound to a_i which is, however, realistic for modern, high-quality welds without large defects such as lack of fusion or similar.

2.7 Multiple crack analyses

At stress levels above the endurance limit, multiple crack propagation is to be expected as the result of the varying local geometry along the weld toe which results in a number of hot spots for crack initiation. In IBESS, the weld toe is subdivided into equidistant partitions. Based on statistically processed scan results of the weld toe, each section is assigned a set of geometry parameters as well as an initial crack (Fig. 7).

Fig. 7 Partitioning of the weld toe into equidistant sections in IBESS [4]
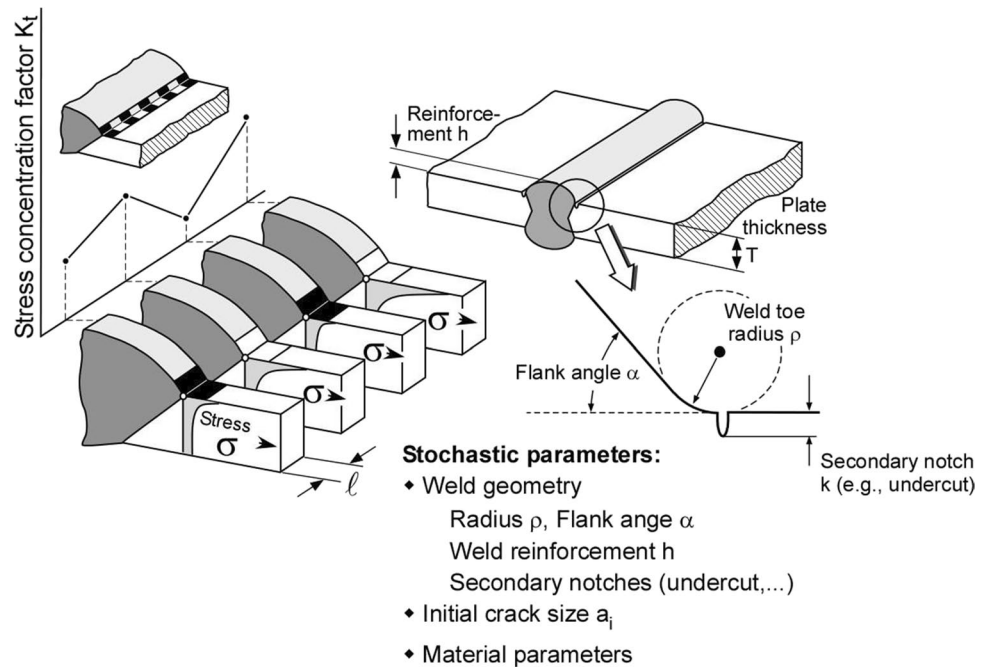
A fatigue crack propagation analysis is carried out simultaneously for all the partitions. Depending on the stress level, it turns out that the cracks grow at different rates and that some of them even arrest. When the surface points of two adjacent cracks touch, crack coalescence is assumed.

If the principle is applied to the finite life branch of the *S–N* curve, the calculations are terminated when a failure criterion (e.g. fracture or a certain crack depth) is met. At each stress level, a number of specimens is simulated. This scheme is repeated at different stress levels. This scatter can be statistically processed for defining *S–N* curves for different percentile values of probability (Fig. 8).

The determination of the endurance limit (also illustrated in Fig. 8) follows a slightly different philosophy. The endurance limit has to be pre-defined, e.g. for no failure up to 10^7 loading cycles. Note that any other value can be chosen, e.g. $N = 2 \times 10^6$, which corresponds to the definition of the FAT class. It has been demonstrated that IBESS, in principle, can be applied to the determination of FAT classes when limit values of the weld geometry are used as the input information [30]. Generally, simulations are performed with a number of specimens at stepwise increased stress levels. The target information of the analysis is the number of failure events per trial at each stress level. Below a certain load only run outs can be stated, above another value 100% failure. In between, the ratio of failures

to the total number of tests can be statistically processed. The result is a probability function of the endurance limit.

3 The application of the methods to selected examples

3.1 The database

The methods are evaluated on the basis of experimental *S–N* curves which have been provided in the IBESS project. From the total of 31 curves, a number of 10 curves have been selected for the present study. This representative selection is summarized in Table 1. The variations included:

Three weldment types (butt welds, cruciform joints and longitudinal gussets).

- Two materials (S355NL and S960QL).

- Different weld geometries generated by MAG and TIG welding.

- As-welded and post-weld heat-treated (PWHT) conditions.

- Testing at different *R* ratios (− 1; 0; 0.5).

With respect to the materials, heat-affected zone (HAZ) tensile properties were required since the fatigue cracks initiated at the weld toes and propagated most of their life through the HAZ. A comprehensive characterization of the materials is found in [3, 4] and shall not be repeated here. Only the hardness profiles across

Fig. 8 Basic principle of the stochastic IBESS analysis for the finite life branch of the $S - N$ curve and the endurance level [4]

Table 1 _S–N_ curves used as dataset for the comparison in this study. The data sets are taken from IBESS [4]

Case	Joint geometry	Material	Condition	_R_ ratio	_f(R)_
A	Butt weld	S355NL	As-welded	− 1	1.3
B	Butt weld	S355NL	PWHT	− 1	1.6
C	Butt weld	S355NL	PWHT	0	1.2
D	Butt weld	S960QL	As-welded	0.5	1
E	Butt weld	S960QL	PWHT	− 1	1.6
F	Cruciform joint	S355NL	PWHT	0	1.2
G	Cruciform joint	S960QL	PWHT	− 1	1.6
H	Cruciform joint	S960QL	PWHT	0	1.2
I	Longitudinal gusset	S355NL	as-welded	0	1
J	Longitudinal gusset	S355NL	PWHT	0	1.2

the weld seams and the associated cyclic stress–strain curves are shown in Figs. 9 and 10. The HAZ micro-structure was martensitic-bainitic for both materials.

4 Application of IBESS to the selected weldments

The aim of the present paragraph is to give to the reader an overview of the input parameters of IBESS; all the details can be found in [4].

The global geometry of the joints and the local weld toe geometrical features are necessary for the calculation of the local stress profiles by means of analytical formulations implemented in IBESS (for butt and cruciform joints). These data are provided for each case study in Figs. 12 to 15. For longitudinal gussets, no analytical solutions for the stress profile are available; thus, the in-depth stress profile has to be input from the user (from a FE analysis for example).

A further geometrical input needed in a fracture mechanics-based analysis is the initial crack shape and size. In IBESS, the initial cracks have been considered semi-circular and the size has been derived from that of micro-notches found at the weld toe. It has been found that the micro-notches were statistically distributed according to a normal or lognormal distribution. In case of the steel S355NL, the average depth was 62 μm with a standard deviation of 17 μm. In case of the steel S960QL instead, the average depth was 29 μm and the standard deviation 7 μm.

Material data such as the cyclic stress–strain curve, the cyclic _R_-curve and the crack propagation curve parameters

Fig. 9 Hardness distributions across the weld seams of the two investigated materials; butt welds [4]
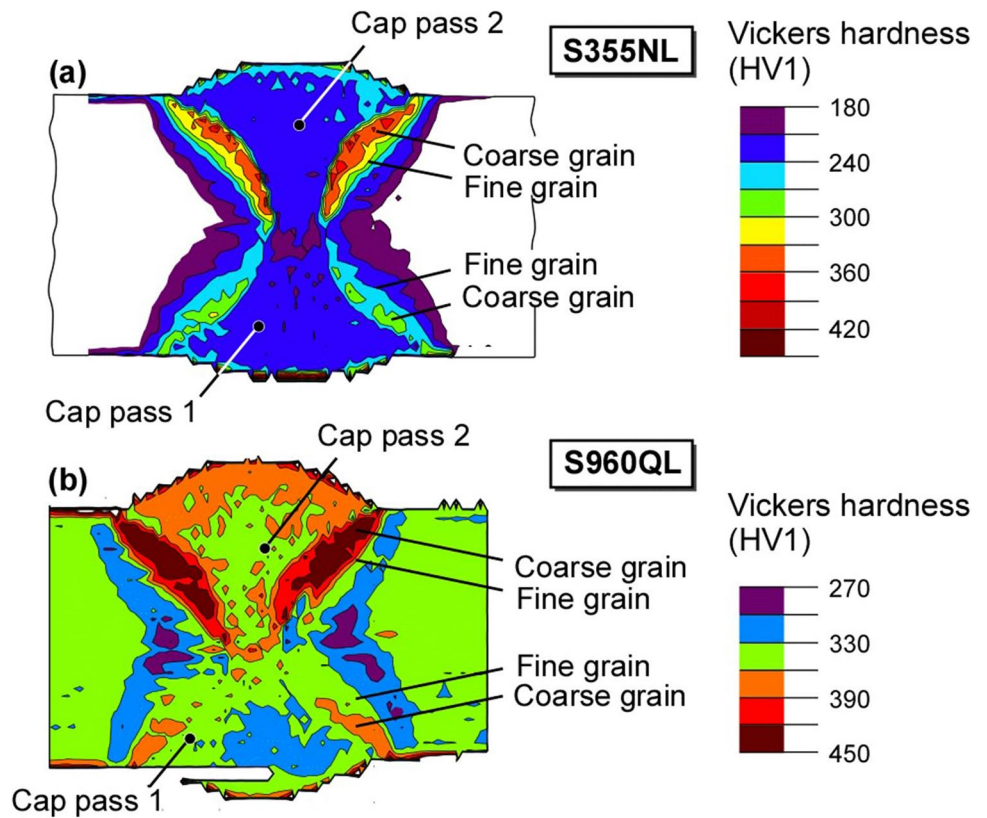
Fig. 10 Cyclic stress–strain curves at different positions of the base metal and HAZ of the two investigated materials [4]

E modulus, all variations: 210 GPa

Material		K' in MPa	n'
S355 Base metal	◐	1203	0.203
S355 HAZ CG CP1	◐	1527	0.170
S355 HAZ CG CP2	◐	1896	0.157
S355 HAZ FG CP1	◆	1539	0.198
S355 HAZ FG CP2	◇	1744	0.195
S960 Base metal	◐	1367	0.089
S355 HAZ CG CP1	◐	1729	0.103
S960 HAZ CG CP2	◐	1838	0.098
S960 HAZ FG CP1	◆	1520	0.127
S960 HAZ FG CP2	◇	1295	0.068
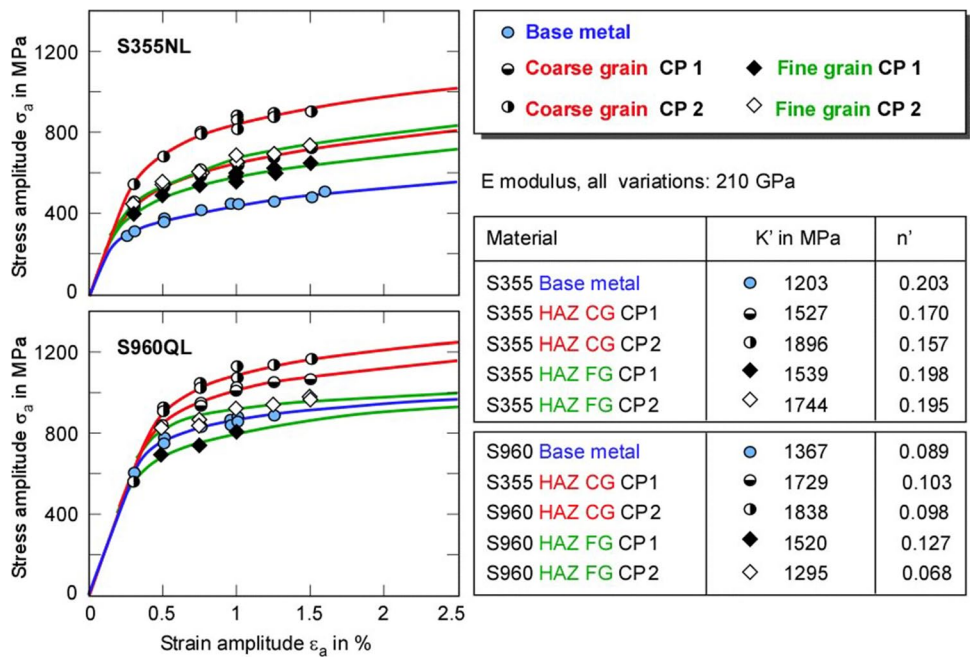
Table 2 Parameters of the crack propagation law implemented in IBESS [4]. The values refer to the $da/dN - \Delta K_{\mathrm{eff}}$ curves, where da/dN is given in mm/cycle and ΔK_{eff} in MPa•m$^{1/2}$

Parameter	S355NL	S960QL
C	0.439×10^{-7}	0.915×10^{-7}
m	2.64	2.21
p	0.8	0.7
$\Delta K_{\mathrm{th,eff}}$	2.7	2.8

must be provided. The fatigue crack propagation within IBESS is described by the following equation:

$$\frac{da}{dN} = C \cdot \left(\Delta K_{\mathrm{eff}} \right)^m \cdot \left[1 - \frac{\Delta K_{\mathrm{th}}(a)}{\Delta K} \right]^p \tag{21}$$

The value of the parameters in Eq. (21) for each material adopted in the IBESS simulations (S355NL and S960QL) is listed in Table 2.

5 Application of the PSM

5.1 Application of the PSM to full penetration butt and cruciform joints

Full penetration butt and cruciform joints have been analysed considering 2D models; in particular, only a quarter model of each geometry has been modelled due to the double symmetry. The 2D geometry has been meshed using 4-node plane elements (PLANE 182) using Ansys® 18.1 software, which enables the user to set the element technology according to four different options by selecting a proper parameter called "K-option 1": (0) full integration method, (1) reduced integration, (2) enhanced strain formulation and (3) simplified enhanced strain formulation.

From Ansys® Mechanical APDL element library, the K-option 1 has been set to 3 (simplified enhanced strain formulation) to be consistent with the original 2D calibration of the PSM [1, 18].

The FE mesh has been generated using the free mesh algorithm of Ansys® by setting the so-called global element size parameter d, i.e. the average finite element size. Since the critical point is the weld toe, only mode I stresses have to be assessed there; the minimum FE mesh density ratio a_{ref}/d must be equal to or greater than 3, a_{ref} being half the main plate thickness, in order to guarantee that $K_{\mathrm{FE}}^* = 1.38 \pm 3\%$ (see Eq. 2) [2]

Referring to Table 3, the plate thickness of the double-sided full penetration butt joints is $T = 10$ mm; thus, the maximum FE size is $d = (10/2)/3 = 1.67$ mm [2]. Since butt joints analysed have a reinforcement height of $h = 1.57$ mm

and $h = 2.02$ mm and an opening angle at the weld toe of 148° and 155°, an element size $d = 1$ mm has been chosen instead of $d = 1.67$ mm in order to have at least 3 elements along the weld flank [31]. Regarding the full penetration cruciform joints, the plate thickness T is 10 mm according to Table 4. The maximum element size for the application of the PSM is again $d = (10/2)/3 = 1.67$ mm; therefore, a global element size $d = 1.5$ mm has been chosen in this case.

Another recommendation for the appropriate application of the PSM with 2D models is that 2 elements must share the node located at the singularity point in the case of $2\alpha > 90°$ [2]. Such condition has been largely verified to be automatically fulfilled by the free-mesh generation algorithm available in Ansys®, and the mesh reported in Table 3 and Table 4 provides confirmation that this condition was met.

Table 3 and Table 4 summarize the PSM parameters adopted for the calculations performed on full-penetration butt and cruciform joints. The last row of each table shows the percentage difference between the $\Delta\sigma_{\mathrm{eq,peak}}$ obtained applying directly Eq. 10 ($\Delta\sigma_{\mathrm{eq,peak,PSM}}$) and obtained calculating the SED from FEM (Eq. 9 with $\Delta\overline{W} = \Delta\overline{W}_{\mathrm{FEM}}$). The difference is higher, the higher is the deviation of the opening angle beyond $2\alpha = 135°$, as highlighted previously in Section 2.2. Table 3 and 4 highlight that the deviation between $\Delta\sigma_{\mathrm{eq,peak,PSM}}$ and $\Delta\sigma_{\mathrm{eq,peak,SED}}$ is in the range 15–22%, because Eq. 10 has been used outside its range of applicability. Therefore, $\Delta\sigma_{\mathrm{eq,peak,SED}}$ has been used in these cases.

The SED in the case of 2D models has been evaluated by means of Ansys® numerical code. Four-node plane elements (PLANE 182) have been adopted with a free mesh having a global size of 0.28 mm as reported in Table 3 and according to recommendations reported in the literature [32].

5.2 Application of the PSM to longitudinal gussets

A 3D, one-eighth of the whole model of the specimen has been defined using the symmetry conditions. The main dimensions of the longitudinal gusset model adopted for the application of the PSM are shown in Table 5. For 3D models, the PSM has been calibrated considering different element types such as 8-node brick, 4-node and 10-node tetra elements [2]. Hereinafter, only the results obtained applying the PSM with 10-node tetra elements (SOLID 187 of Ansys® library) will be shown. Differently from 2D FE models, in 3D models meshed with tetra elements, the variation of number of tetra vertexes sharing a node along the weld toe line must be taken into account [2, 17]. Therefore, a simple engineering approach has been adopted, which consists in using a moving average of peak stresses evaluated at three adjacent vertex nodes, named $s - 1$, s and $s + 1$ [2].

Table 3 Double-sided, full-penetration butt-welded joints geometries and 2D 4-node quadrilateral element FE model for the application of the PSM

Joint geometry			FE model according to the PSM		

B (mm)	T (mm)	L (mm)	h (mm)	2α (°)	ρ (mm)
360	10	12.80	1.57	148	0
360	10	13.62	2.02	155	0

FE results - $2\alpha = 148°$

PSM parameters for $2\alpha = 148°$		PSM parameters for $2\alpha = 155°$	
Material	Steel	Material	Steel
E	206000 MPa	E	206000 MPa
ν	0.3 -	ν	0.3 -
Constants for f_{w1} calculation		*Constants for f_{w1} calculation*	
2α	148 °	2α	155 °
λ_1	0.740 -	λ_1	0.784 -
e_1	0.105 -	e_1	0.098 -
R_0	0.28 mm	R_0	0.28 mm
K_{FE}^*	1.38 -	K_{FE}^*	1.38 -
Mesh		*Mesh*	
Half plate thickness $T/2$	5 mm	Half plate thickness $T/2$	5 mm
$d_{max} - (T/2)/3$	1.7 mm	$d_{max} - (T/2)/3$	1.7 mm
d	1 mm	d	1 mm
Stresses		*Stresses*	
$\Delta\sigma_{peak}/\Delta\sigma_{nom}$	1.45 -	$\Delta\sigma_{peak}/\Delta\sigma_{nom}$	1.44 -
f_{w1}	0.923 -	f_{w1}	0.844 -
$\Delta\sigma_{eq,peak,PSM}/\Delta\sigma_{nom}$	1.34 MPa	$\Delta\sigma_{eq,peak,PSM}/\Delta\sigma_{nom}$	1.21 MPa
d_{SED}	0.28 mm	d_{SED}	0.28 mm
$\Delta\sigma_{eq,peak,SED}/\Delta\sigma_{nom}$	1.61 MPa	$\Delta\sigma_{eq,peak,SED}/\Delta\sigma_{nom}$	1.56 MPa
Difference % *	-17 %	Difference %*	-22 %

*Difference% $= (\Delta\sigma_{eq,peak,PSM} - \Delta\sigma_{eq,peak,SED})/\Delta\sigma_{eq,peak,SED} \cdot 100$

$$\overline{\Delta\sigma}_{ij,peak,n=s} = \frac{\Delta\sigma_{ij,peak,s-1} + \Delta\sigma_{ij,peak,s} + \Delta\sigma_{ij,peak,s+1}}{3} \quad (22)$$

Having in hands the average peak stress range relative to node n, the equivalent peak stress range is calculated again by means of Eq. 10, simply by substituting the peak stress ranges $\Delta\sigma_{ij,peak}$ with the average peak stress ranges $\overline{\Delta\sigma}_{ij,peak}$ (Eq. 22). A summary of all parameters adopted for the PSM application to longitudinal gussets is reported in Table 5.

Longitudinal gusset dimensions have been taken from [33], and the typical weld seam of longitudinal gussets tested is shown in Fig. 11. It is seen that the opening angle at the weld toe is equal to $2\alpha = 146°$, which was determined by means of experimental measurements. It is worth mentioning that the upper weld toe of all longitudinal gussets has been hammer-peened to avoid crack initiation there.

As a result of the FE stress analysis, the percentage difference between the $\overline{\Delta\sigma}_{eq,peak,PSM}$ and the $\overline{\Delta\sigma}_{eq,peak,SED}$ resulted equal to -6%. The small error obtained in this case justifies the use of Eq. 10, without the need for evaluating the SED from dedicated FE analyses.

The SED in the case of 3D models has been evaluated by means of Ansys® numerical code. Ten-node tetra elements (SOLID 187) have been adopted with a free mesh having a global size of 1.5 mm and a local size of 0.07 mm inside the control volumes as reported in Table 5. Indeed, the weld toe line has been divided into small control volumes along its length having both radius and height equal to 0.28 mm in order to analyse the distribution of the averaged SED parameter.

5.3 Applied loads and boundary conditions

For butt, cruciform and longitudinal joints, a tensile stress equal to 1 MPa has been applied to the main plate, as shown in Tables 3, 4 and 5, respectively. Symmetry boundary conditions have then been applied to appropriate edges of 2D (or surfaces for the 3D) models.

5.4 Postprocessing of FE analyses

Starting from the FAT class according to the PSM (PSM FAT = 156 MPa, relative to $N_A = 2 \times 10^6$ loading cycles and to a survival probability of 97.7%; see Fig. 3), the FAT class in terms of range of the applied nominal stress (PSM FAT$_{nom}$) can be calculated as follows:

$$\text{PSM FAT}_{nom} = \frac{\text{PSM FAT}}{\Delta\sigma_{eq,peak,PSM}/\Delta\sigma_{nom}} \rightarrow = \frac{156\ MPa}{\Delta\sigma_{eq,peak,PSM}/\Delta\sigma_{nom}} \quad (23a)$$

$$\text{PSM FAT}_{nom} = \frac{\text{PSM FAT}}{\Delta\sigma_{eq,peak,SED}/\Delta\sigma_{nom}} \rightarrow = \frac{156\ MPa}{\Delta\sigma_{eq,peak,SED}/\Delta\sigma_{nom}} \quad (23b)$$

where it is worth mentioning that Eq. 23a has been used for longitudinal gussets, while Eq. 23b has been applied for butt and cruciform joints.

The postprocessing followed for the longitudinal gusset was slightly different, because in this case, both weld toe and weld root have been analysed. In particular, at the weld toe, only mode I contribution has been considered in Eq. 10, while at the weld root, all modes (i.e. opening, sliding and tearing) have been taken into account.
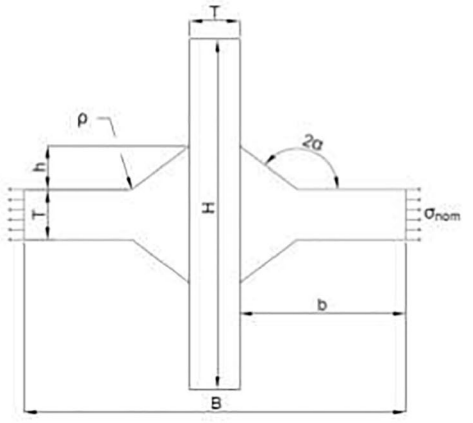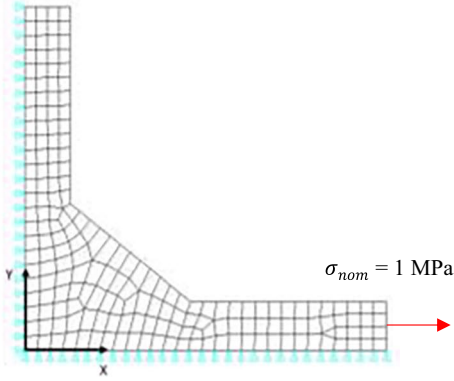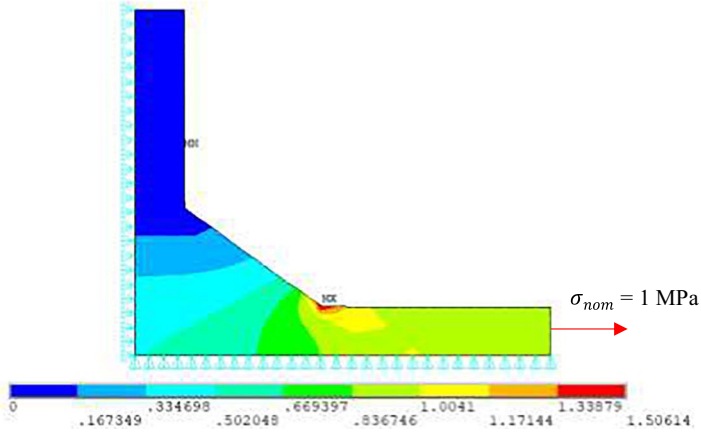
By using Eqs. 23a and 23b, the experimental data in terms of nominal stress range $\Delta\sigma_{nom}$ vs number of cycles to failure N_f can be compared with the PSM estimations.

5.5 Case study A: butt weld of S355NL, as-welded condition, R = −1

The experimental *S–N* data and the estimations of PSM and IBESS, together with the FAT class according to IIW, are given in Fig. 12a. In Fig. 12b, IBESS simulations are shown whereby the mean curves are shown in addition to the 97.7 percentile curves of IBESS and PSM. Moreover, the IIW FAT class curve referred to $R = -1$ by Eq. 1b (enhancement factor $f(R) = 1.3$, with $R = -1$) relative to the 97.7% probability of survival is shown.

Some considerations can be obtained from the figure. While a slope of $k = 3$ of the fatigue curves is pre-implemented in the PSM, the slope regarding IBESS is a result of the analysis. What shows up is a slope of approximately $k = 3$ in the upper part of the IBESS curve, but the curve becomes flatter at low values towards the endurance limit which was predefined for $N = 10^7$ in the present case. Instead of a sharp knee, IBESS predicts a smooth transition. Another eye-catching difference concerns the scatter band. In the PSM, the scatter index $T_\sigma = 1.90$ is fixed, while in IBESS, the scatter is the result of probabilistic simulations in which the geometrical parameters are randomly extracted from their probability density functions. In the present case, 10 simulations have been performed at each stress level which consequently result in 10 $(\Delta\sigma, N)$ points. The data can then be processed statistically. In comparison with the experiment, the scatter band appears to be too large in PSM and too small in IBESS. The PSM scatter band is larger than the IBESS one since the same PSM band is valid for different weldments given that the original scatter band has been obtained considering the results of T-joints and cruciform fillet–welded joints showing weld toe failures. The reason for the small scatter band in IBESS is the omission of the scatter in the $da/dN - \Delta K$ data, i.e. the mean value of the parameter C of the crack propagation law has been

Table 4 Full-penetration cruciform welded joint geometry and 2D 4-node quadrilateral element FE model for the application of the PSM

Joint geometry				FE model according to the PSM		
B (mm)	b (mm)	H (mm)	T (mm)	h (mm)	2α (°)	ρ (mm)
360	175	70	10	8.72	143	0

FE results

PSM parameters for $2\alpha = 143°$		
Material	Steel	
E	206000	MPa
ν	0.3	-
Constants for f_{w1} calculation		
2α	143	°
λ_1	0.713	-
e_1	0.110	-
R_0	0.28	mm
K_{FE}^*	1.38	-
Mesh		
Half plate thickness $T/2$	5	mm
$d_{max} = (T/2)/3$	1.7	mm
d	1.5	mm
Stresses		
$\Delta\sigma_{peak}/\Delta\sigma_{nom}$	1.51	-
f_{w1}	1.098	-
$\Delta\sigma_{eq,peak,PSM}/\Delta\sigma_{nom}$	1.65	MPa
d_{SED}	0.20	mm
$\Delta\sigma_{eq,peak,SED}/\Delta\sigma_{nom}$	1.95	MPa
Difference % *	-15	%

[*]$\text{Difference}\% = (\Delta\sigma_{eq,peak,PSM} - \Delta\sigma_{eq,peak,SED})/\Delta\sigma_{eq,peak,SED} \cdot 100$

considered. The assessment of a realistic order of magnitude for this and the implementation in IBESS is subject of ongoing work. Note that PSM predicts a constant scatter in double-logarithmic scale along the finite life branch of the *S–N* curve while the scatter becomes larger towards the endurance limit in IBESS.

What is not shown in the figure is the simulation of the FAT class by IBESS. This has been done according to the method for determining the endurance limit described in Section 2.3.4 but with the $N = 5 \cdot 10^6$ limit. The result is a IBESS FAT class of 193 MPa. The corresponding value of the PSM (named PSM FAT$_{nom}$) is 100 MPa, that of IIW but corrected for $R = -1$ is 104 MPa (all results calculated at 97.7% probability of survival and 2×10^6 cycles), as Fig. 12b shows.

The experiments of case A have been carried out on butt welds in the as-welded condition. Consequently, PSM takes into account welding residual stresses by means of the mean stress correction parameter $c_w = 1$ (Eq. 11). In IBESS, residual stresses are neglected although the as-welded residual stresses were available as through-wall as well as surface profiles from measurements and finite element simulations [3, 34]. However, it turned out (a) that they were negligible at the position of the weld toe and (b) experiments and finite element simulations demonstrated that existing residual stresses (tension as well as bending) would disappear due to cyclic loading at a stress ratio of $R = -1$ [3, 34]. Therefore, the IBESS analysis without considering residual stresses makes sense for configurations such as the data set of case A.

At higher *R* ratios, cyclic loading has a similar effect. Finite element simulations even point to the build-up of compressive residual stresses. However, a discrepancy with experimental results is apparent from various reasons which will not be discussed here (but see [3, 34]). As a consequence of this evidence, IBESS provides some guidance of how to treat residual stresses in fatigue crack propagation analyses but recommends their omission at the present state of the approach. This at least provides conservative assessments.

5.6 Further case studies: B to E

The results of the PSM and IBESS analyses of the four cases including the materials S355NL and S960QL in as-welded and PWHT state and at *R* ratios of − 1, 0 and 0.5 are shown along with the experimental data in Fig. 13. Only the mean curve of the finite life branch of the predicted *S–N* curve is shown. It shows up that, different to case A, PSM tends to overestimate the experimental fatigue strength in case B. Comparing Figs. 12a and 13a, experimental data do not show a noticeable difference, although in the former case, weldments were in the as-welded state, while in the latter, they were PWHT. According to Eq. 11, the PSM

for the PWHT state and $R = -1$ adopts a mean stress correction parameter $c_w = 0.5$. This has the effect to increase PSM curves towards higher stress ranges of a factor equal to $1/\sqrt{0.5} = 1.41$ according to Eq. 10. This justifies the higher PSM curve of the PWHT case B with respect to the as-welded case A. For other cases, the PSM agrees with experimental data.

IBESS provides better predictions with the exception of data set C where it showed up to be conservative. The authors suspect that $R = 0$ might be the reason. In Section 3.4, it was mentioned that there is some indication that the cyclic loading could lead to compressive residual stresses at the weld toe. It has been also mentioned that further work is required to be certain about this. Let us, for the moment, assume that there are really compressive stresses. What would be the consequence? The real stress ratio, which the crack tip experiences, would be lower than the nominal one for which the IBESS analyses were carried out. In other words, the loading conditions assumed in the analysis have been harsher than in reality. Therefore, the predicted *S–N* curve has been shifted to lower *N* values.

This immediately brings up the question why a similar trend is not observed for case D where the *R* ratio has been even 0.5. A possible explanation is the higher yield strength of the HAZ material of the S960QL steel (cases D and E) when compared with S355NL (cases A–C) (Figs. 12 and 13). Residual stress relaxation is caused by local plastic deformation. Whether and to what extent this will occur depends on the stress concentration at the weld toe and, of course, also on the yield strength of the material. The higher the latter is, the lower the probability of extended plasticity. Note that this explanation is still a speculation which needs further investigations.

5.7 Further case studies: cruciform joints of data sets F to H

In this section, one cruciform joint of S355NL (case F) and two of S960QL (cases G and H) are investigated. The former is loaded with $R = -1$ and the latter with $R = 0$. According to Fig. 14, the PSM gives conservative results for data set F and G, while it seems to slightly overestimate the *S–N* curve for data set H.

Except for case H, where results are in agreement with the PSM, IBESS tends to underestimate the experimental *S–N* curves, even for $R = -1$. It is important to understand that the method uses two-dimensional influence or weight functions for the determination of the *K* factor which then is plasticity-corrected. In any case, the stress profile in wall thickness direction refers to the real component while the geometry function of the *K* factor solution is provided for a substitute geometry, in the present case a flat plate. Analytical solutions implemented in IBESS for such substitute

Table 5 Longitudinal gusset geometry and 3D 10-node tetra element FE model for the application of the PSM

Longitudinal gusset: main dimensions								
B (mm)	H (mm)	T (mm)	h (mm)	l (mm)	w (mm)	z (mm)	2α (°)	ρ (mm)
150	50	10.2	7.7	75	50	11.4	146	0

Equivalent peak stress ranges for weld toe and root

$\Delta\sigma_{eq,peak} = 1.32\ MPa$ ROOT

$\Delta\sigma_{eq,peak} = 2.34\ MPa$ LOWER TOE

PSM parameters adopted for weld toe		
Mesh: 10-node tetra elements		
LOWER TOE - Mode I - $2\alpha = 146°$		
Material	Steel	
E	206000	MPa
ν	0.3	-
Constants for f_{w1} calculation		
2α	146	°
λ_1	0.729	-
e_1	0.107	-
R_0	0.28	mm
K_{FE}^*	1.21	-
Mesh		
$a_{ref} = T / 2$	5.1	mm
$d_{max} = a_{ref} / 3$	1.7	mm
d	1.5	mm
Stresses		
$\Delta\sigma_{peak}/\Delta\sigma_{nom}$	2.53	MPa
f_{w1}	0.925	-
$\Delta\sigma_{eq,peak,PSM}/\Delta\sigma_{nom}$	2.34	MPa
d_{SED}	0.07	mm
$\Delta\sigma_{eq,peak,SED}/\Delta\sigma_{nom}$	2.48	MPa
Difference %	-6	%

PSM parameters adopted for weld root			
Mesh: 10-node tetra elements			
	Mode I	Mode II	Mode III
Material	Steel		
E	206000 MPa		
ν	0.3		
Constants for f_{wi} calculation			
2α	0°		
λ_1	0.5		
e_1	0.133	0.340	0.414
R_0	0.28 mm		
$K_{FE}^*, K_{FE}^{**}, K_{FE}^{***}$	1.05	1.63	1.37
Mesh			
$a_{ref} = min\ (l,h,T/2)$	min (75, 7.7, 5.1) = 5.1 mm		
$d_{max} = a_{ref} / 3$	1.7 mm		
d	1.5 mm		
Stresses			
f_{w1}, f_{w2}, f_{w3}	1.314	3.261	3.025
$\Delta\sigma_{eq,peak,PSM}/\Delta\sigma_{nom}$	1.32 MPa		

Fig. 11 Longitudinal gusset weld seam [4]

geometry provide conservative estimations of stress intensity factors; this is one of the reasons why IBESS predictions are conservative (at least for case F and case G).

5.8 Further case studies: longitudinal gussets of data sets I and J

In this section, two data sets of longitudinal gussets of S355NL are considered which are loaded at $R = 0$ (Fig. 15). One set of specimens has been tested in the as-welded condition; the other has been post-weld heat treated. The experimental data reveal a common observation on this type of geometries: that there is not much difference between these conditions for R ratio equal to 0 [35]. A difference compared to the butt welds and cruciform joints considered in the previous sections is that no reaction or long-range residual stresses did exist there. This is different for longitudinal gussets which are restrained in themselves. As a consequence, residual stresses of some 10% of the yield strength have been measured at the weld toe of the longitudinal gussets [3, 34]

which seem the crack to keep open. That the IBESS predictions are nonetheless conservative is probably the result of the difference in stiffness between the component and the substitute geometry for K factor determination such as discussed in Section 3.6. Therefore, although IBESS finally yields conservative predictions, the situation is unsatisfactory.

Longitudinal gussets have been hammer-peened in correspondence to the upper weld toe. This has been done to avoid the crack to start from the upper weld toe and to induce the failure from the lower weld toe. The PSM let to determine what is the most critical point regarding the initiation of the crack by comparing equivalent average peak stress ranges $\overline{\Delta\sigma}_{\text{eq,peak}}$ at the weld toe and weld root, respectively. As shown in Table 5, the equivalent peak stress range $\overline{\Delta\sigma}_{\text{eq,peak}}$ at the weld toe is 2.34 MPa while at the weld root is 1.32 MPa. Since the $\overline{\Delta\sigma}_{\text{eq,peak}}$ of the weld toe is bigger than at the weld root, the PSM predicts that the failure occurs at the weld toe. Indeed, this is confirmed by experimental results. By analysing Fig. 15, it emerges that the PSM is slightly conservative with respect to experimental data, providing however acceptable results.

6 Conclusions

This work aimed at comparing the IBESS and the PSM approaches for the fatigue life assessment of welded joints. The approaches have been tested against ten case studies comprising different geometries (butt welds, cruciform joints and longitudinal gussets), two steels with different strength (S355NL and S960QL), two residual stress conditions (as-welded and post-weld heat treated) and three stress ratios (− 1, 0 and 0.5). In all cases, the well-established IIW FAT nominal stress approach has been considered for comparison.

Fig. 12 Estimated *S–N* curves for butt welded joints (case A) according to PSM and IBESS and comparison with FAT class according to IIW [5]. **a** Experimental data, PSM and IBESS fatigue curves for 50% survival probability. **b** PSM and IBESS fatigue curves for 50% and 97.7% survival probability
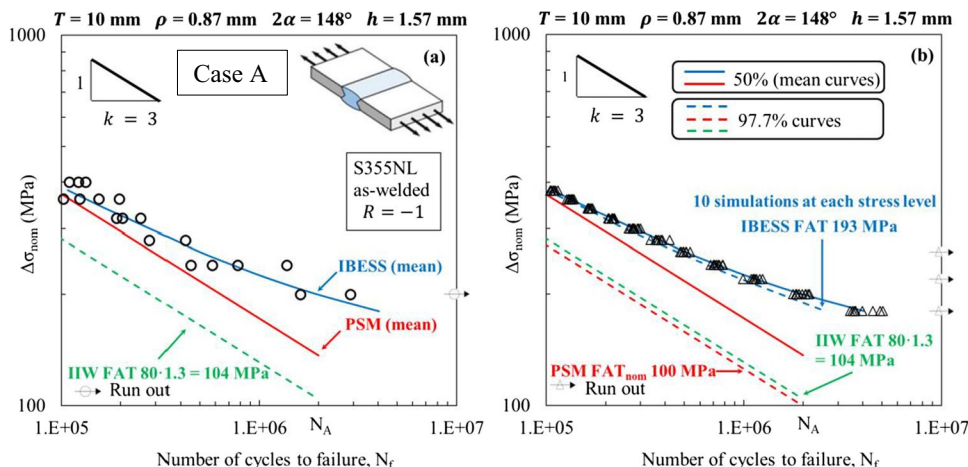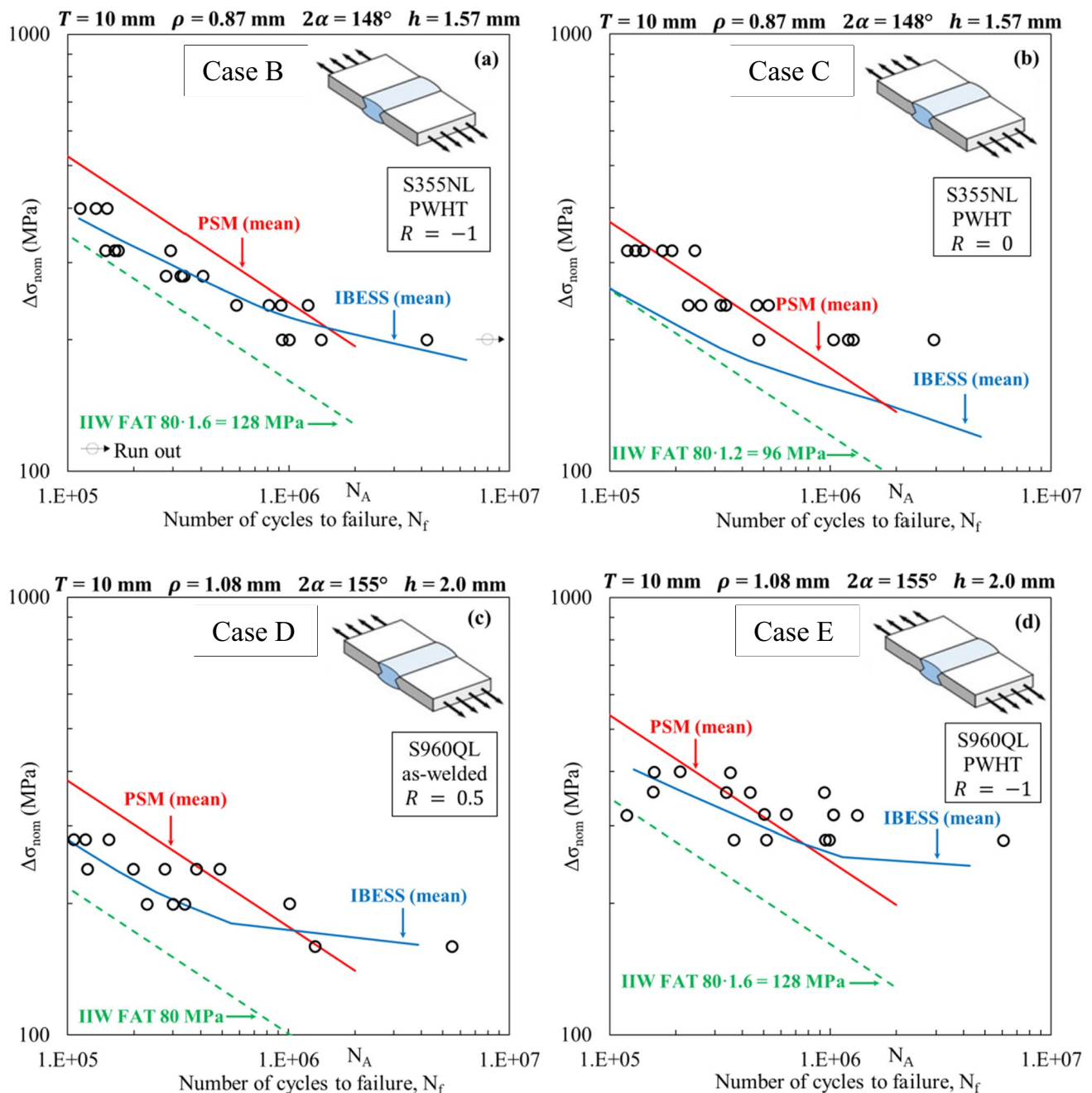
Fig. 13 Estimated *S–N* mean fatigue curves for butt welded joints according to PSM and IBESS and comparison with FAT class according to IIW [5]. **a** Case B; **b** case C; **c** case D; **d** case E

The comparison has some significance because the approaches are based on different philosophies. While the PSM is an engineering FE-oriented technique which relies on coarse FE models for the rapid evaluation of the NSIFs at the weld toe and weld root, which are idealised as sharp V-notches, and on the SED approach for the fatigue modelling, the IBESS approach is based on fracture mechanics, considering short and long fatigue crack propagations. The

underlying philosophies and working hypotheses result in the following advantages and drawbacks:

- The PSM has been calibrated on a large experimental dataset of welded joints. Therefore, it considers a fixed slope of the *S–N* curve ($k = 3$) and a fixed scatter index ($T_\sigma = 1.90$) independent of joint geometry, steel strength and testing conditions. On the contrary, in the IBESS approach, the slope and the scatter band are the results of

Fig. 14 Estimated *S–N* mean fatigue curves for cruciform joints according to PSM and IBESS and comparison with FAT class according to IIW [5]. **a** Case F; **b** case G; **c** case H
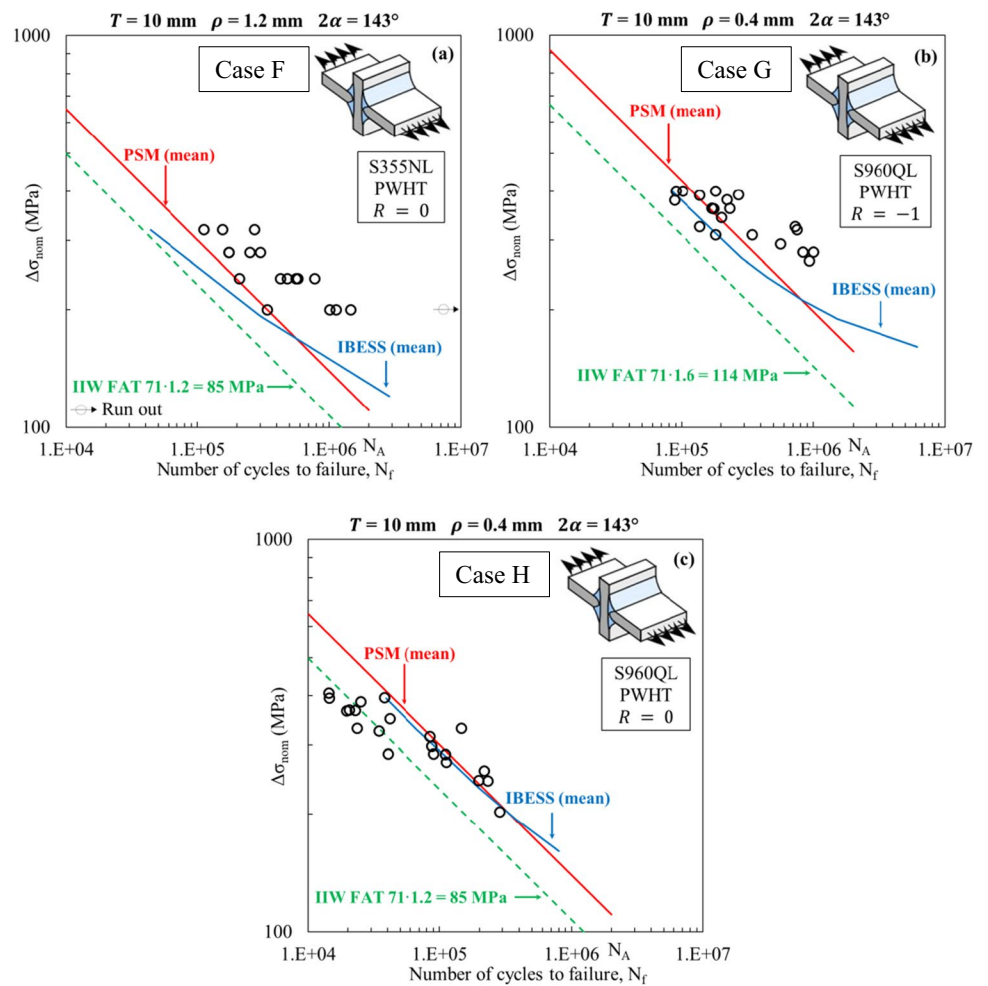
Fig. 15 Estimated *S–N* mean fatigue curves for longitudinal gussets according to PSM and IBESS and comparison with FAT class according to IIW [5]. **a** Case I; **b** case J
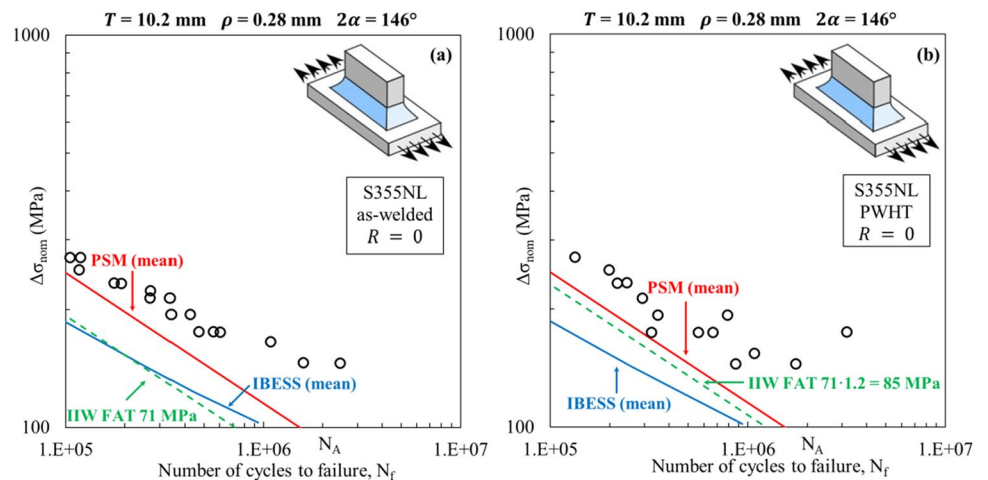
fracture mechanics-based probabilistic simulations which are specific to each case study.

- The PSM can be applied to a wider range of geometries and load cases as the NSIFs are calculated via FE models for weld root and weld toe, whereas IBESS suffers at the present state from limitations given by the weight functions solutions and reference yield stress solutions implemented for the calculation of the plasticity-cor-

rected stress intensity factors. Furthermore, IBESS does not apply to weld root failures.

- In contrast, IBESS considers the large scatter of the local geometrical parameters along the weld toe and it can deal with multiple crack propagation by a geometrical partition of the weld seam. This is not the case for the PSM approach, in which the weldment is modelled by average geometrical values.

- The IBESS model can predict the fatigue limit as non-propagating condition of the simulated cracks (all the cracks simultaneously simulated in a multiple crack propagation analysis are arrested), whereas the PSM provides a technical definition of the fatigue limit, i.e. the stress level for a given number of cycles technically considered as runout (typically 2×10^6 or 10^7).

In light of the previous statements, the results can be interpreted as follows:

- In case of butt welds, good predictions of the mean *S–N* curve are provided by IBESS, except for $R = 0$, for which the PSM approach works better. The IBESS approach can predict fairly good also the fatigue limit, but it shows a too narrow scatter band because material parameters have been considered deterministic.

- The PSM provided better predictions than IBESS for cruciform joints. The authors suspect that this is mainly due to the analytical solutions implemented in IBESS which provide conservative estimates of the stress intensity factors for this type of joint and therefore conservative fatigue life predictions.

- This problem has been magnified for the simulations of the longitudinal gussets, where no specific analytical solutions were available. Furthermore, the in-depth residual stress profile was not considered in the simulations carried out with IBESS. This led to overconservative predictions, whereas the PSM was closer to the experimental results.

- In general, the IIW FAT classes showed always conservative estimates.

The comparison with the experimental results pointed out areas of improvement for both approaches. The range of analytical solutions implemented in IBESS should be extended, and information about realistic in-depth profiles of residual stresses and scatter of the crack propagation data is needed to improve the fatigue life predictions. Concerning the PSM approach, the conditions of applicability in terms of geometrical parameters should be extended, in particular to weld toe angles $2\alpha > 135°$. Indeed, for the longitudinal gussets, the PSM was successfully used even though the weld toe angle was $2\alpha = 146°$. However, for the butt and cruciform joints, the PSM could not be applied outside its range of applicability and the FE determination of the SED has been necessary in order to obtain the equivalent peak stress with good accuracy. For further improving the PSM, an estimation of the fatigue limit of different welded joint geometries should be included.

References

1. Meneghetti G, Lazzarin P. Significance of the elastic peak stress evaluated by FE analyses at the point of singularity of sharp V-notched components. Fatigue Fract Eng Mater Struct 2007;30. https://doi.org/10.1111/j.1460-2695.2006.01084.x.

2. Meneghetti G, Campagnolo A (2020) State-of-the-art review of peak stress method for fatigue strength assessment of welded joints. Int J Fatigue 139:105705. https://doi.org/10.1016/j.ijfatigue.2020.105705

3. Zerbst U, Savaidis G, Beier HT. Special issue on fracture mechanics-based determination of the fatigue strength of weldments. Eng Fract Mech 2018;198.

4. Zerbst U, Madia M, Schork B, Hensel J, Kucharczyk P, Ngoula D, et al. Fatigue and fracture of weldments. The IBESS approach for the determination of the fatigue life and strength of weldments by fracture mechanics analysis. Cham: Springer International Publishing; 2019. https://doi.org/10.1007/978-3-030-04073-4.

5. Hobbacher AF. Recommendations for fatigue design of welded joints and components. IIW Collection. Springer International Publishing; 2016. https://doi.org/10.1007/978-3-319-23757-2.

6. Eurocode 3 . Eurocode 3: design of steel structures – part 1–9: Fatigue. CEN; 2005.

7. Rennert D, Kullig E, Vormwald M, Esderts A, Siegele D. Analytical strength assessment of components made of steel, cast iron and aluminium materials in mechanical engineering. FKM Guidel. 6th ed., Frankfurt/Main, Germany: Forschungskuratorium Maschinenbau (FKM); 2013.

8. Kaffenberger M. Schwingfestigkeit von Schweißverbindungen und Übertragbarkeit von Schweißverbindungswöhlerlinien. Report No. 97. (in German). 2012.

9. Williams ML (1952) Stress singularities resulting from various boundary conditions in angular corners of plates in tension. J Appl Mech 19:526–528

10. Qian J, Hasebe N (1997) Property of eigenvalues and eigenfunctions for an interface V-notch in antiplane elasticity. Eng Fract Mech 56:729–734. https://doi.org/10.1016/S0013-7944(97)00004-0

11. Gross B, Mendelson A (1972) Plane elastostatic analysis of V-notched plates. Int J Fract Mech 8:267–276. https://doi.org/10.1007/BF00186126

12. Lazzarin P, Tovo R (1998) A notch intensity factor approach to the stress analysis of welds. Fatigue Fract Eng Mater Struct 21:1089–1103. https://doi.org/10.1046/j.1460-2695.1998.00097.x

13. Meneghetti G. The use of peak stresses for fatigue strength assessments of welded lap joints and cover plates with toe and root failures. Eng Fract Mech 2012;89. https://doi.org/10.1016/j.engfracmech.2012.04.007.

14. Meneghetti G. The peak stress method for fatigue strength assessment of tube-to-flange welded joints under torsion loading. Weld World 2013;57. https://doi.org/10.1007/s40194-013-0022-x.

15. Meneghetti G, Guzzella C. The peak stress method to estimate the mode I notch stress intensity factor in welded joints using three-dimensional finite element models. Eng Fract Mech 2014;115. https://doi.org/10.1016/j.engfracmech.2013.11.002.

16. Campagnolo A, Roveda I, Meneghetti G (2019) The peak stress method combined with 3D finite element models to assess the fatigue strength of complex welded structures. Procedia Struct Integr 19:617–626. https://doi.org/10.1016/j.prostr.2019.12.067

17. Campagnolo A, Meneghetti G. Rapid estimation of notch stress intensity factors in 3D large-scale welded structures using the peak stress method. MATEC Web Conf., vol. 165, 2018. https://doi.org/10.1051/matecconf/201816517004.

18. Meneghetti G, Campagnolo A, Avalle M, Castagnetti D, Colussi M, Corigliano P, et al. Rapid evaluation of notch stress intensity factors using the peak stress method: comparison of commercial finite element codes for a range of mesh patterns. Fatigue Fract Eng Mater Struct 2018;41. https://doi.org/10.1111/ffe.12751.

19. Livieri P, Lazzarin P (2005) Fatigue strength of steel and aluminium welded joints based on generalised stress intensity factors and local strain energy values. Int J Fract 133:247–276. https://doi.org/10.1007/s10704-005-4043-3

20. Lazzarin P, Livieri P, Berto F, Zappalorto M (2008) Local strain energy density and fatigue strength of welded joints under uniaxial and multiaxial loading. Eng Fract Mech 75:1875–1889. https://doi.org/10.1016/j.engfracmech.2006.10.019

21. Lazzarin P, Zambardi R (2001) A finite-volume-energy based approach to predict the static and fatigue behavior of components with sharp V-shaped notches. Int J Fract 112:275–298. https://doi.org/10.1023/A:1013595930617

22. Fischer C, Fricke W, Rizzo CM (2016) Review of the fatigue strength of welded joints based on the notch stress intensity factor and SED approaches. Int J Fatigue 84:59–66. https://doi.org/10.1016/j.ijfatigue.2015.11.015

23. Meneghetti G, Lazzarin P. The peak stress method for fatigue strength assessment of welded joints with weld toe or weld root failures. Weld World 2011;55.

24. Haibach E. Service fatigue-strength – methods and data for structural analysis. Dusseldorf: VDI; 1989.

25. R6, Revision 4. Assessment of the integrity of structures containing defects. EDF Energy, Barnwood, Gloucester; 2014.

26. BS7910. Guide to methods for assessing the acceptability of flaws in metallic structures. The British Standards Institution (BSI) Standards Publ., London; 2019.

27. Suresh S. Fatigue of materials. 2nd ed. Cambridge University Press; 2003. https://doi.org/10.1017/CBO9780511806575.

28. NASGRO, Fatigue crack growth computer program "NASGRO" Version 3 2019.

29. Maierhofer J, Kolitsch S, Pippan R, Gänser H-P, Madia M, Zerbst U (2018) The cyclic R-curve – determination, problems, limitations and application. Eng Fract Mech 198:45–64. https://doi.org/10.1016/j.engfracmech.2017.09.032

30. Schork B, Zerbst U, Kiyak Y, Kaffenberger M, Madia M, Oechsner M (2020) Effect of the parameters of weld toe geometry on the FAT class as obtained by means of fracture mechanics-based simulations. Weld World 64:925–936. https://doi.org/10.1007/s40194-020-00874-7

31. Meneghetti G, Campagnolo A, Berto F. Fatigue strength assessment of partial and full-penetration steel and aluminium butt-welded joints according to the peak stress method. Fatigue Fract Eng Mater Struct 2015;38. https://doi.org/10.1111/ffe.12342.

32. Lazzarin P, Berto F, Zappalorto M (2010) Rapid calculations of notch stress intensity factors based on averaged strain energy density from coarse meshes: theoretical bases and applications. Int J Fatigue 32:1559–1567. https://doi.org/10.1016/j.ijfatigue.2010.02.017

33. Zerbst U. Analytische bruchmechanische Ermittlung der Schwingfestigkeit. Final Report of IBESS Subproject A3 (in German). 2016.

34. Hensel J, Nitschke-Pagel T, TchoffoNgoula D, Beier H-TT, Tchuindjang D, Zerbst U (2018) Welding residual stresses as needed for the prediction of fatigue crack propagation and fatigue strength. Eng Fract Mech 198:123–41. https://doi.org/10.1016/j.engfracmech.2017.10.024

35. Hensel J, Nitschke-Pagel T, Dilger K (2017) Engineering model for the quantitative consideration of residual stresses in fatigue design of welded components. Weld World 61:997–1002. https://doi.org/10.1007/s40194-017-0467-4